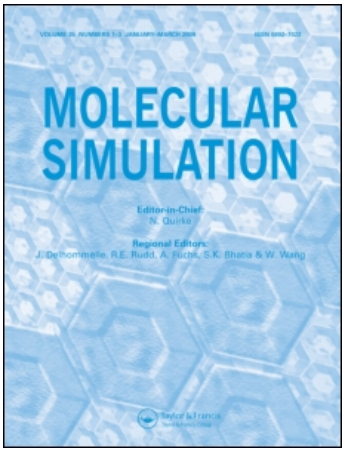

Molecular Simulation
Publication details, including instructions for authors and subscription information:
http://www.informaworld.com/smpp/title~content=t713644482

Nanoindentation response of nickel surface using molecular dynamics simulation

Wen-Yang Chang[a]; Te-Hua Fang[b]; Shiang-Jiun Lin[c]; Jian-Jin Huang[d]
[a] Microsystems Technology Center, Industrial Technology Research Institute, Tainan, Taiwan, R.O.C. [b] Department of Mechanical Engineering, National Kaohsiung University of Applied Sciences, Kaohsiung, Taiwan, R.O.C. [c] Department of Mold and Die Engineering, National Kaohsiung University of Applied Sciences, Kaohsiung, Taiwan, R.O.C. [d] Institute of Mechanical and Electromechanical Engineering, National Formosa University, Yunlin, Taiwan, R.O.C.

Online publication date: 15 October 2010

To cite this Article Chang, Wen-Yang , Fang, Te-Hua , Lin, Shiang-Jiun and Huang, Jian-Jin(2010) 'Nanoindentation response of nickel surface using molecular dynamics simulation', Molecular Simulation, 36: 11, 815 — 822
To link to this Article: DOI: 10.1080/08927021003677761
URL: http://dx.doi.org/10.1080/08927021003677761

Molecular Simulation
Vol. 36, No. 11, September 2010, 815–822

Taylor & Francis
Taylor & Francis Group

Nanoindentation response of nickel surface using molecular dynamics simulation

Wen-Yang Chang[a], Te-Hua Fang[b]*, Shiang-Jiun Lin[c] and Jian-Jin Huang[d]

[a]*Microsystems Technology Center, Industrial Technology Research Institute, Tainan 709, Taiwan, R.O.C.* [b]*Department of Mechanical Engineering, National Kaohsiung University of Applied Sciences, Kaohsiung 807, Taiwan, R.O.C.* [c]*Department of Mold and Die Engineering, National Kaohsiung University of Applied Sciences, Kaohsiung 807, Taiwan, R.O.C.* [d]*Institute of Mechanical and Electromechanical Engineering, National Formosa University, Yunlin 632, Taiwan, R.O.C.*

(*Received 5 November 2009; final version received 4 February 2010*)

The mechanisms of dislocation nucleation on a nickel (Ni) (001) surface under nanoindentation behaviours are investigated using molecular dynamics simulation. The characteristic mechanisms include the molecular models of a thermal layer (TL) and thermal with a free layer (TFL), multi-step load/unload cycles, tilt angles and shapes of the indenter, and slip vectors. The model of a TL has higher reaction force than a TFL. The maximum forces of nanoindentation decrease with increasing time of the multi-step load/unload cycle. The indenter with the tilt angle has larger force to act on the molecular model than the indenter along the normal direction. The effect of the indentation shape is presented such that the conical tip has larger load force to act on the molecular model. The defects along Shockley partials on the (111) plane are produced during nanoindentation involving nucleation, glide and slip.

Keywords: nanoindentation; molecular dynamics; multi-step load/unload; tilt angle; slip vector

1. Introduction

Nanotechnology plays a key role in engineering reliability for investigating the mechanical characteristics of material behaviours at the atomic scale [1,2]. Recently, nanoindentation [3,4] and nanoscratch [5,6] experiments have been widely performed to measure Young's modulus and hardness of a variety of materials. Experimental tests reveal *in situ* practical, mechanical and processing responses of nanomaterials, but they are unsuitable for investigating the defect and deformation-induced mechanisms at the atomic scale. Nanoindentation experiment is challenging because it is difficult to vertically indent the sample without changing the tilt angle of the indenter. The effect of the tilt angle of the indenter is difficult to obtain from experiments. Understanding the detailed mechanisms of atomistic deformation is a fundamental challenge in material science.

However, molecular dynamics (MD) simulation for nanotechnology analyses of atomistic models has been used to further clarify the dislocation and defect structures [1,2]. The MD method can be effective in simulating the atomistic characteristics of deformation and microscopic fracture processes, and offering insights into microscopic behaviours. The deformation mechanism of ultra-hard carbide layer under nanoindentation [7] and the dislocation nucleation in various orientations at the surface of the nickel (Ni) single crystals [8] were investigated using MD simulation. Although the mechanisms of onset plasticity, dislocation nucleation and elastic–plastic deformation [9–12] have recently been investigated using MD simulation, few studies have focused on dynamic nanoindentation [13,14]. The phenomenon of the indenter's tilt angle is more meaningful and interesting to study using MD simulation.

The phenomena of various molecular models, the multi-step load/unload cycle, the deformation mechanism of atoms, tilt angles and shapes of the indenter, and slip vectors were investigated using MD simulation at the surface of the Ni single crystals. For the various models of MD simulation, the thermal layer (TL) and thermal with a free layer (TFL) were used to analyse the mechanism of surface plasticity. The effects of the maximum loads at the maximum depths of dynamic nanoindentation were investigated. The multi-step load/unload cycles of nanoindentation with different depths, shapes and tilt angles of the indenter were investigated. The aim of this study is to provide further insight into the dynamic characteristics of the Ni atoms on the nanoindentation mechanism.

2. MD simulation

The models of a TL and a TFL, as shown in Figure 1, were used to investigate the mechanical behaviour and the underlying mechanism of surface plasticity for obtaining a satisfactory molecular model. During the MD simulation processes, the TL atoms remained at a constant temperature, indicating that all atomic heat is uniform after the heat is induced by the indenter. All atoms in the free layer are independent and can vary their temperatures,

*Corresponding author. Email: fang.tehua@msa.hinet.net

ISSN 0892-7022 print/ISSN 1029-0435 online

DOI: 10.1080/08927021003677761
http://www.informaworld.com

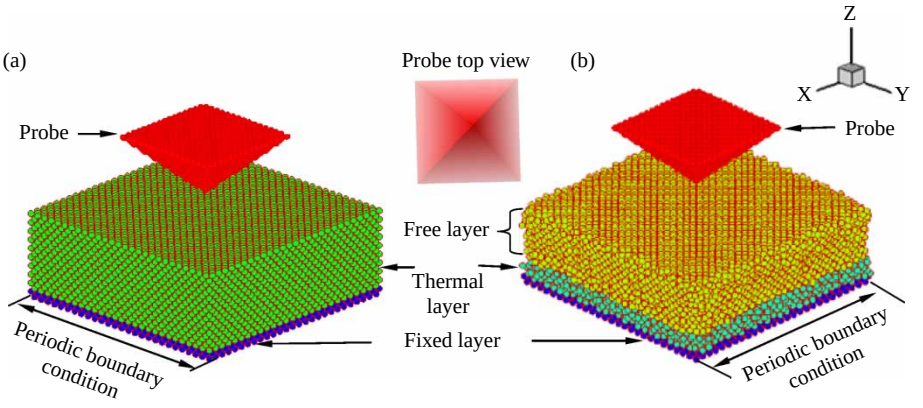

Figure 1. Models for MD simulations: (a) TL and (b) TFL.

meaning that the temperature depends on the friction force between the indenter and the atoms. Two model sizes in the x, y and z directions are 10.93, 10.93 and 4.86 nm, respectively, using a face-centred-cubic (FCC) bulk crystal. The indenter was a Vickers probe consisting of 2992 diamond atoms in the form of a square-based pyramid with an angle of 22° between the indenter face and the contact surface. The indenter was assumed to be a rigid probe during the simulation process. The model was initially assumed to have a well-defined atomic structure before thermal equilibration. The indented surface was the (001) plane of Ni single crystals for all the numerical experiments. The periodic boundary conditions of the sample were used in the transverse directions. The bottom of the models, two layers of atoms, was fixed in space to prevent the substrate from being moved. The velocities of the atoms of the thermal control layers are given by the Maxwell–Boltzmann distribution [15] of the prescribed substrate temperature. Periodic boundary conditions were enforced in the x and y directions; there is no periodic boundary condition along the z direction. The position of the incident atoms was random in the x and y directions, and the z direction of the incident atoms was at 20-fold lattice length above the substrate surface. The boundary condition of the temperature at the TL and TFL is initially at a temperature of 300 K. The indenter was moved at a constant speed of 100 ms^{-1} for load/unload cycles of the nanoindentation process. The model is equilibrated to its minimum energy configuration at a temperature of 300 K.

For the MD simulation, the model was evaluated by integrating the Newtonian equations of motion using a Verlet algorithm method [16] with a time step of 1 fs. The force acting on an individual atom was obtained by summing the forces contributed by the surrounding atoms. The Morse two-body potential and the second-moment approximation of the tight-binding many-body (TB-SMA) potential were adopted to model the atomic interactions among the Ni atoms. The Morse potential considers only the interaction between two atoms without including the simultaneous influence of their neighbouring atoms. The Morse potential energy, $U_{\mathrm{Morse}}(r_{ij})$, can be described with three parameters as

$$U_{\mathrm{Morse}}(r_{ij}) = D\left(\mathrm{e}^{-2\alpha(r_{ij}-r_0)} - 2\mathrm{e}^{-\alpha(r_{ij}-r_0)}\right), \qquad (1)$$

where D, r_0 and r_{ij} are the cohesion energy of exchange interaction, the equilibrium distance and the separation distance between atoms i and j, respectively. α is fitted to the bulk modulus of the material. For Ni–C atoms, the values of D, α and r_0 are 1.0094 eV, 0.19875 nm^{-1} and 0.256 nm, respectively.

The TB-SMA potential, $U(r_{ij})$, contains a repulsive pair potential and a cohesive band energy term as follows:

$$U(r_{ij}) = \sum_{i=1}^{N}\left[-\left[\sum \xi^2 \exp\left(-2q\left(\frac{r_{ij}}{r_0}-1\right)\right)\right]^{1/2} + \sum_j A\exp\left[-p\left(\frac{r_{ij}}{r_0}-1\right)\right]\right], \qquad (2)$$

where ξ, r_0 and N are the effective hopping integral, the first-neighbour distance, and the number of atoms considered, respectively. ξ, q, p and A are fitted to the experimental values of cohesive energy. For Ni atoms, the values of ξ, q, p, r_0 and A are 1.07 eV, 1.189, 16.999, 0.2491 nm and 0.0376 eV, respectively.

For the adhesive force, the contact pressure applied by the indenter was calculated using formula (3):

$$P_{\mathrm{c}} = \frac{\sum_{i\in\Psi} F_i}{24.56\times\left(h_{\max} - \chi\times\left(\sum_{i\in Z} F_i/S\right)\right)^2}, \qquad (3)$$

where Ψ represents all atoms of the film belonging to the contact zone; F_i is the out-of-balance force on the atom i; $h_{\max}$ and S are the maximum indentation depth and unloading stiffness, respectively; and χ is the geometric constant of the indenter, $\chi = 0.75$ for the Vickers probe.

3. Results and discussion

3.1 Effect of molecular models

After nanoindentation of the MD simulation, the force vs. depth relationships for the TL and TFL models are shown in Figure 2. The maximum forces for the TL model at maximum depths of 0.77, 1.15, 1.44 and 1.73 nm are 0.97, 2.48, 4.83 and 6.48 mN, respectively. After curve fitting, the force for the TL model at a depth of 1.15 nm is lower. The maximum forces for the TFL model at maximum depths of 0.77, 1.15, 1.44 and 1.73 nm are 0.79, 1.57, 2.23 and 2.49 mN, respectively. The stiffness of the TL model, the force divided by depth dF/dh, is higher than that of the TFL model. The force for both TL and TFL models at a nanoindentation depth of 0.8 nm is similar; however, the force difference for the TL and TFL models increases with increasing nanoindentation depth. Obviously, the interatomic bonding forces are relatively weak in the TFL model because the atoms have more freedom and vibrational energy than those in the TL model. For the TL model, the stress at the contact area was high when the indenter gradually reached the substrate surface. However, for the TFL model, the atoms in the adjustable temperature layer depend on the friction force between the probe and the atoms.

The nanoindentation velocities vs. load force relationships for the TL and TFL models at a temperature of 300 K are shown in Figure 3. The maximum forces for the TL model at velocities of 96, 105, 118 and 125 m/s are 0.51, 1.11, 1.90 and 2.47 mN, respectively. The maximum forces for the TFL model at velocities of 96, 105, 118 and 125 m/s are 0.70, 1.51, 2.90 and 4.16 mN, respectively. For both models, the maximum forces linearly increased with increasing nanoindentation velocities. This is due to larger structural recovery with increasing nanoindentation velocities. The recovery was governed by the dislocation and slip mechanism. The forces for the TL model were higher than those for the TFL model as the nanoindentation velocity was increased. The TL model had larger friction force and larger deformation during nanoindentation. The forces in internal atoms increased with increasing indentation depth or velocity.

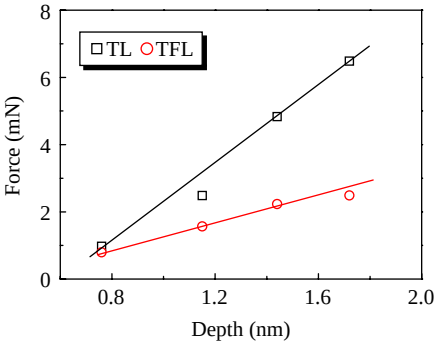

Figure 2. Relationship between the force and depth for the TL and TFL models.

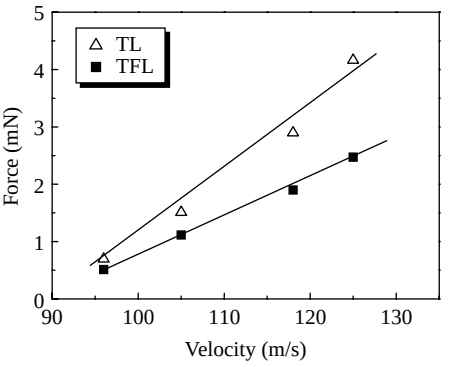

Figure 3. Nanoindentation velocity vs. force relationship at a temperature of 300 K for the TL and TFL models.

3.2 Multi-step load/unload cycle

The multi-step load/unload cycles with three repetitions at maximum depths of 0.76, 1.15, 1.44 and 1.72 nm were investigated for dynamic behaviours of the TL model, as shown in Figure 4(a). The maximum forces increased with increasing indentation depth, but the forces gradually decreased with an increasing number of load/unload cycles. The elastic energy and stiffness increased with increasing indentation depth. The decreasing forces representing the elastic energy of the surface were overcome when the multi-step load/unload cycle was increased. This result is similar to that of the reported literature [17]. There is a jump-contact phenomenon [18] when the indenter begins to approach the Ni surface. The indenter surface has a potential energy that attracts the Ni atoms. There is also a small stress drop that produced homogeneous slip planes in defect structures due to the surface relaxation of atoms. The phenomenon of the stress drop nearly disappeared with an increasing number of load/unload cycles [19,20]. It was predicted that the plastic deformation of MD was induced by dislocation slipping at the first nanoindentation. After the indenter was gradually released from the Ni film, Ni atoms were almost separated from the indenter. The data presented that Ni atoms did not adhere in the vicinity of the indenter tip and had good structural recovery for elastic deformation.

The maximum forces of each load/unload cycle with three repetitions at maximum depths of 0.76, 1.15, 1.44 and 1.72 nm for the TL and TFL models are shown in Figure 4(b). The trend of curves for both the models is similar, but the maximum forces at each load/unload cycle of the TFL model are smaller than those of other forces in the TL model. For example, the maximum forces of the TL model for a load/unload cycle with three repetitions

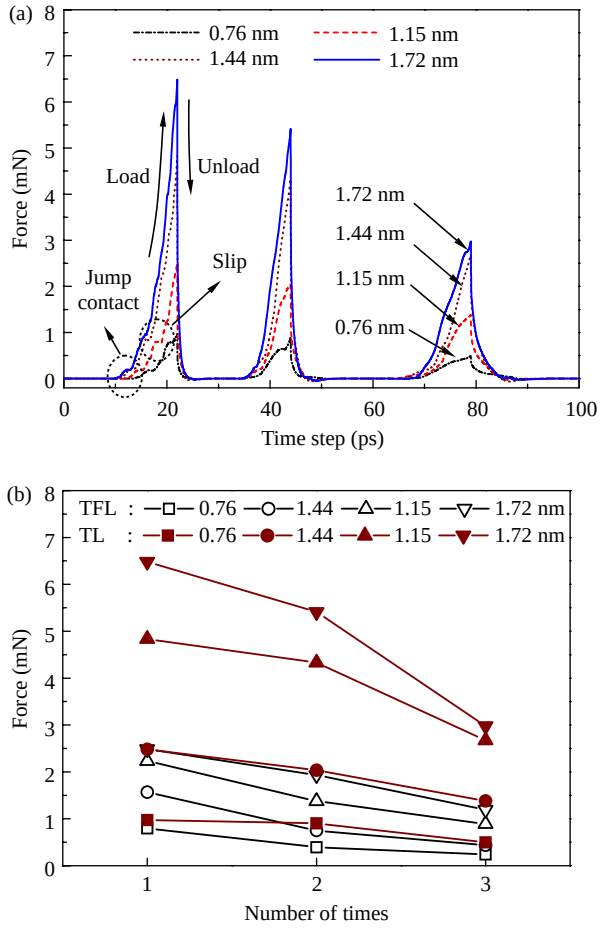

Figure 4. Dynamic behaviours of the multi-step load/unload cycle with three repetitions at maximum depths of 0.76, 1.15, 1.44 and 1.72 nm: (a) TL model and (b) the maximum forces at each load/unload cycle.

at a nanoindentation depth of 1.72 nm are 6.48, 5.41 and 2.87 mN, respectively. The maximum forces of the TFL model for a load/unload cycle with three repetitions at the nanoindentation depth of 1.72 nm are 2.49, 1.93 and 1.19 mN, respectively. The maximum forces for each load/unload cycle decreased with an increasing number of indentations due to the dislocation and the defect structures formed after the initial indentation. The indenter easily indented the molecular surface to the maximum depth at the next indentation test.

3.3 Dislocation and slip vector

During deformation processes, the partial side views of the indentation and releasing of the Vickers indenter are shown in Figure 5(a) and (b) for the TL model, respectively, and Figure 5(c) and (d) for the TFL model, respectively. As the indentation depth is increasing, the rupture region initiated from a perfect crystalline is induced by the indenter. The atoms of amorphous disordered debris were piled up around the indented region and a clear side flow on the lateral side of the indenter was found when the indenter reached the maximum depth, as shown in Figure 5(a) and (c). Some defects, such as vacancies, slips, dislocations and plastic indents, can be identified by the evolution of the displacement variation of the indenter. A higher degree of plastic deformation took place after nanoindentation. The indentation shape is formed according to the indenter geometry, with atoms being displaced to the periphery of the contact, as shown in Figure 5(b) and (d). For the molecular fluctuation of the maximum indentation, the TFL model had larger deformation near the side flow than the TL model, meaning that the interatomic bonding forces are relatively strong in the TL model. The atoms of the TFL model have higher vibrational energy and mobility within its structure than in the TL model.

The top-view atomic configuration of the plastic groove for the TL model after Vickers indentation is shown in Figure 6(a). The TFL model was not presented because it is similar to the TL configuration. A debris pile-up along the dimple fringe and an amorphous structure around the dimple fringe were found. The gliding of a prismatic dislocation loop mediated permanent deformation far away from the contact surface. The maximum width of the glide bands on the interface of $\{111\}\langle 110\rangle$ slip systems was about 1 nm at an angle of 45°. Based on the dislocation theory, the slip systems in the Ni lattice were the (111) plane along the $[\bar{1}\bar{1}2]$ direction and the $(\bar{1}\bar{1}1)$ plane along the $[\bar{1}\bar{1}\bar{2}]$ direction. In the Thompson tetrahedron notation, the perfect dislocation of Burger's vectors of the two Shockley partials was presented as $\overline{C\delta}$ and $\overline{D\gamma}$, respectively, as shown in Figure 6(b). The (111) planes were stacked on a closely packed sequence ABCABC. Dislocations of the opposite sign on the same slip plane attracted each other, run together and annihilate each other. There is a tendency for the two Shockley partials to separate, creating a region of a stacking fault between them. The normal ABCABC stacking then changed to an ABCACABC stacking, since a B layer glided into the C-position. Therefore, the two Shockley partials, splitting up into two partial dislocations, can be written as $b_1 = b_2 + b_3$,

$$\frac{1}{3}[\bar{1}\bar{1}0] \rightarrow \frac{1}{6}[\bar{1}\bar{1}\bar{2}] + \frac{1}{6}[\bar{1}\bar{1}2]. \tag{4}$$

According to Frank's rule, the repulsive force between the two Shockley partials can be approximated by (5)

$$F_r = \frac{\mu(b_2 \cdot b_3)}{2\pi d}, \tag{5}$$

where d is the spacing between the two Shockley partials and μ is the shear modulus of the material.

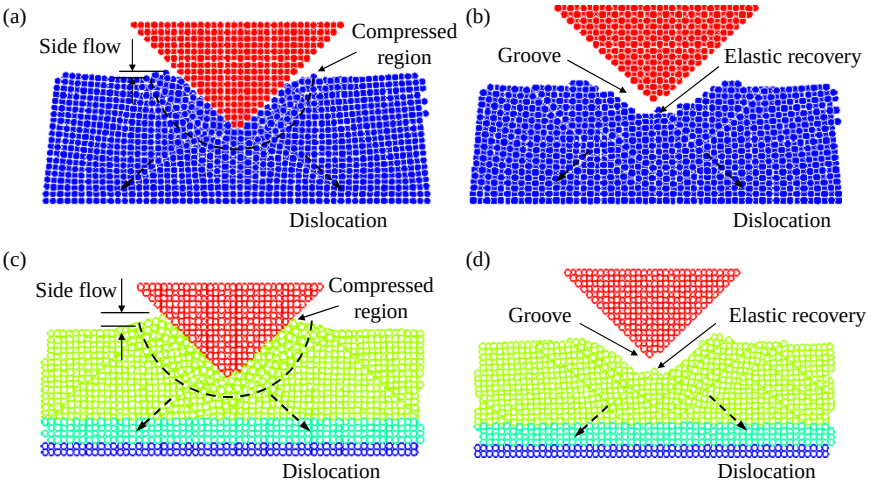

Figure 5. Partial side view of MD behaviour during nanoindentation processes: (a) TL at the maximum indentation depth, (b) TL indenter releasing, (c) TFL at the maximum indentation depth and (d) TFL after indenter releasing.

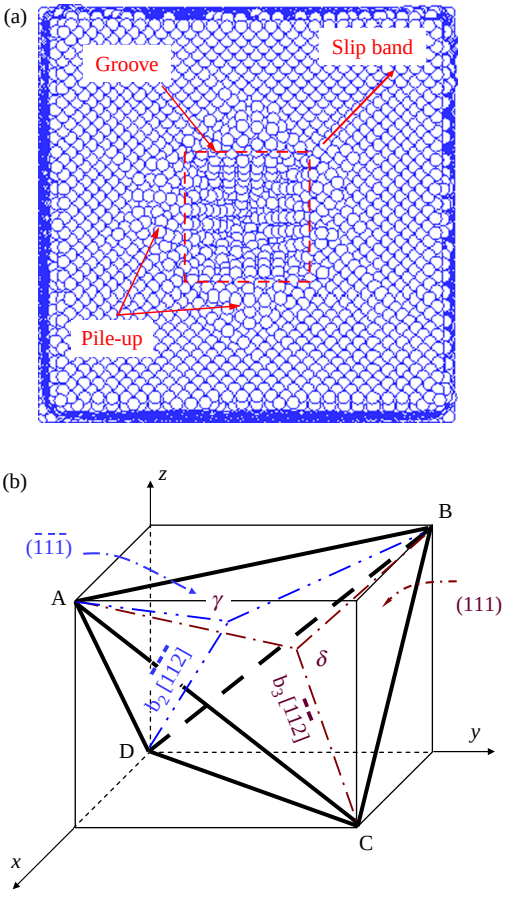

Figure 6. Structures of dislocation nucleation: (a) top-view atomic configurations and (b) schematic diagram of two Shockley partial dislocations.

This study used slip vector analysis to identify and characterise the dislocations being nucleated during nanoindentation. The slip vector approach was first applied to MD studies of nanoindentation by Zimmerman et al. [18]. The slip vector for atom i was defined as

$$s_i = -\frac{1}{n_s}\sum_{j\neq i}^{n}(p_{ij} - R_{ij}), \tag{6}$$

where n_s is the number of slipped neighbours, and p_{ij} and R_{ij} are the vector differences in linking atom i and all its n nearest neighbours j at the current and reference configurations, respectively. The spatial distribution of the slip vector moduli $|s_i|$ around the nanoindentation trace for the TFL model is shown in Figure 7. The TL model was not presented because the trend of the slip vectors was similar. The slip distances included the nanoindentation depths of 7.7, 11.5, 14.4 and 16.3 Å. The colour indicates the slip distances of Ni atoms in angstroms. Green atoms correspond to the values of the slip vectors between the stacking fault value and zero, while red and blue atoms have a slip vector ranging between a complete lattice parameter and the stacking fault value. The dislocation loops nucleated on the four (111) planes and extended into the solid. The sunken shapes in the middle, forming a square-based pyramidal defect structure, were at the maximum depth of indentation. The pyramidal defect structure of FCC was in excellent agreement with the experimentally observed permanent deformation structures [21]. The corresponding slip vector of the atoms on one of the slip planes was (111). The dislocation nucleated on the (111) plane was therefore the $1/6[\bar{1}\bar{1}2]$ Shockley partial. Similarly, $1/6[\bar{1}\bar{1}\bar{2}]$ was nucleated on the plane $(\bar{1}\bar{1}1)$. Therefore, there were low-energy sessile stair-rod dislocations in the pyramid of intrinsic stacking faults on (111) planes. The sessile stair rods act as barriers to gliding, giving rise to the observed strain hardening during nanoindentation beyond the first yield.

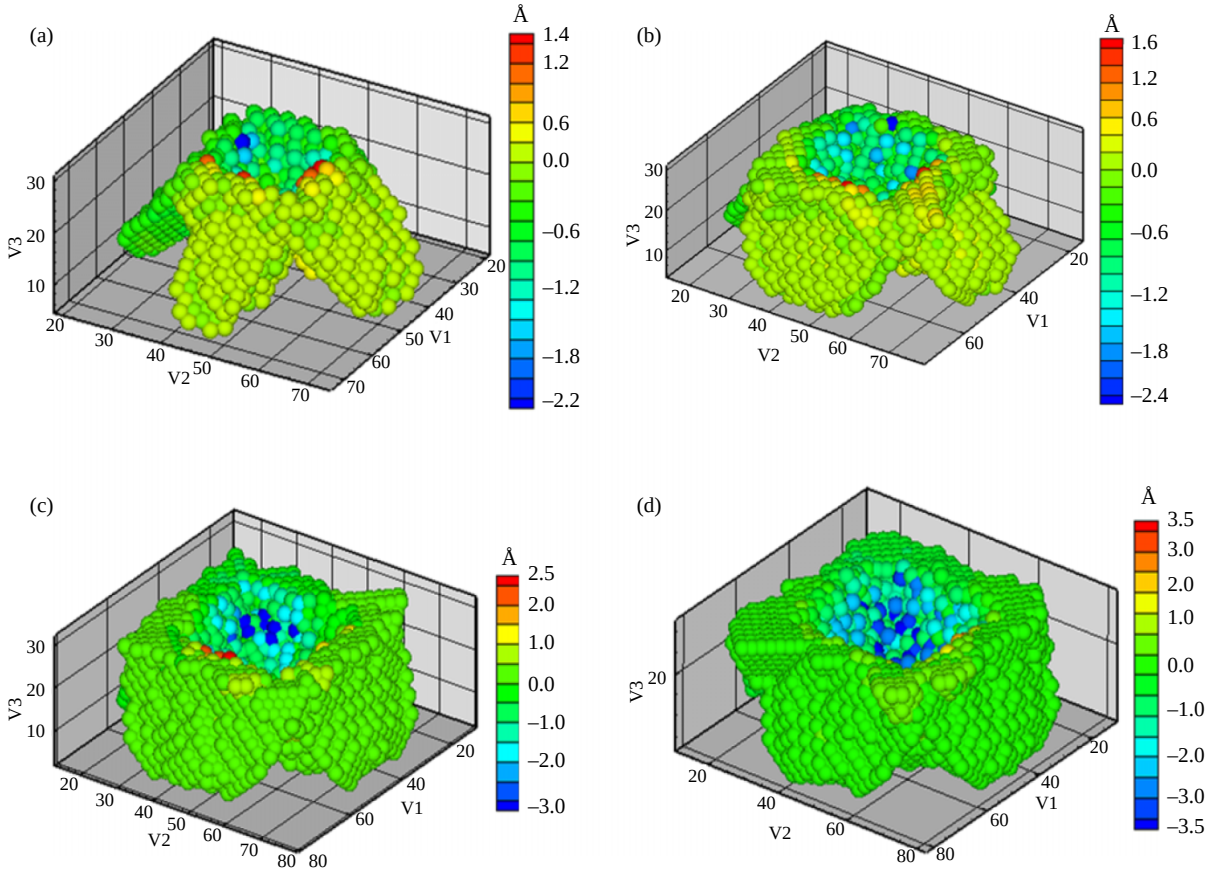

Figure 7. Slip vectors of Ni atoms at a nanoindentation depth of (a) 7.7 Å, (b) 11.5 Å, (c) 14.4 Å and (d) 16.3 Å (colour online).

3.4 Tilts and shapes of the indenter

The tilt angles and shapes of the indenter influence the indentation force and the contact areas during the experimental nanoindentation test. Therefore, it is better to study the effect of the indenter's tilt angle and shape using the MD simulation. The tile angles of the indenter included 0°, 5°, 10°, 15° and 30° at an indentation depth of 0.76 nm. The multi-step load/unload curves with three repetitions at different tilt angles of the indenter for the TL model are shown in Figure 8. Results showed that a force applied along the normal direction, a tilt angle of 0°, produced a smaller reaction force on the surface atoms. The force increased with an increasing tilt angle of the indenter. This was due to the contact area between the indenter and the sample increasing with an increasing tilt angle of the indenter. For example, the maximum forces at the tilt angles of 0°, 5°, 10°, 15° and 30° at the first load/unload cycle were 0.97, 1.16, 1.34, 1.28 and 3.86 mN, respectively. The maximum forces decreased with an increasing number of indentations, indicating that the dislocation and the defect structures of the molecular model were induced by shifted atomic planes after the initial indentation. The indenter then easily indented on

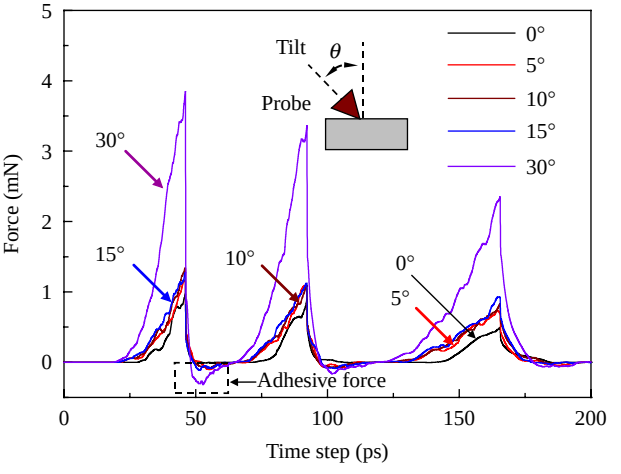

Figure 8. Multi-step load/unload cycle with three repetitions for the TL model with the indenter's tilt angles of 0°, 5°, 10°, 15° and 30° at an indentation depth of 0.76 nm.

the molecular surface at the next indentation. A stress that is normal to the slip plane is greater for homogeneous dislocation nucleation in a single crystal. The Ni atoms

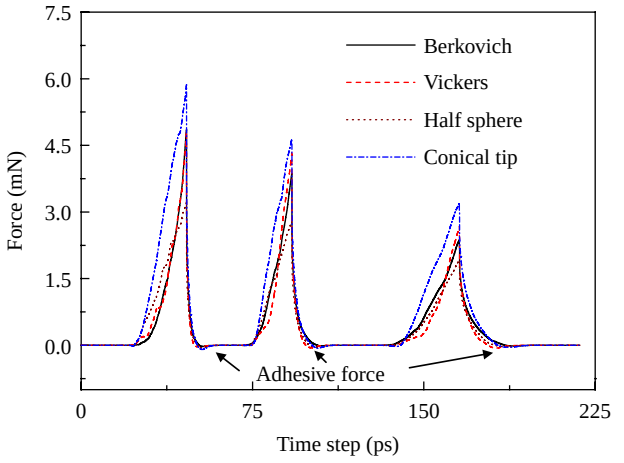

Figure 9. Multi-step load/unload cycle with three repetitions for the TL model using the Berkovich, Vickers, half-sphere and conical tip of indenters.

easily adhered in the vicinity of the indenter tip with an increasing tilt angle of the indenter.

The force reaction of MD varies not only with the tilt angles of the indenter tips but also with the geometrical shapes of the indenter tips in measurement, the former is more significant. The shapes of the indenter included the Berkovich, Vickers, half-sphere and conical tip. The characteristic curves of the multi-step load/unload cycles with three repetitions for the TL model are shown in Figure 9. When comparing the results of the four indenters, the obtained levels for load/unload cycles are highest for the conical tip and lowest for the half-sphere. It was expected that the indentation force at which the substrate started to deform plastically is sensitive to the conical tip. This was due to the contact area between the indenter and the sample. The nanoindentation force increased when the shape of the indenter is smoother. All indenters slightly induced the adhesive forces between the probe and the sample's surface atoms.

4. Conclusions

The multi-step load/unload cycles on the Ni atoms were investigated in order to attain better understanding of the influence of the models, the tilt angles and geometry on the material's behaviour under nanoindentation. The Ni material had dislocation slip lines on the (111) plane along the $[\bar{1}\bar{1}2]$ direction and the $(\bar{1}\bar{1}1)$ plane along the $[\bar{1}\bar{1}\bar{2}]$ direction. The nucleation was split into pairs of Shockley partial dislocations, giving rise to peculiar configurations at the surface of hillocks. Dislocation caused a minor force drop in the load/unload cycle curve. The nanoindentation force in the normal direction has a smaller force component that acts on the surface atoms. A debris pile-up along the dimple fringe and an amorphous structure around the dimple fringe were found. The applied force increased with an increasing tilt angle of the indenter. The nanoindentation force increased when the shape of the indenter is smoother. The effects of the tilt angles and the shape of the indenters should be considered for nanoindentation experiment.

Acknowledgements

This work was partially supported by the National Science Council of Taiwan, under grant no. NSC 96-2628-E-150-005-MY3.

References

[1] D. Mulliah, S.D. Kenny, and R. Smith, *Modeling of stick-slip phenomena using molecular dynamics*, Phys. Rev. B 69 (2004) 205407.
[2] N.Q. Vo, R.S. Averback, P. Bellon, S. Odunuga, and A. Caro, *Quantitative description of plastic deformation in nanocrystalline Cu: Dislocation glide versus grain boundary sliding*, Phys. Rev. B 77 (2008) 134108.
[3] B.L. Oscar, H. Mark, B. Avi, and J.M. Phil, *A simple nanoindentation-based methodology to assess the strength of brittle thin films*, Acta Mater. 56 (2008), pp. 1633–1641.
[4] W.Y. Chang, T.H. Fang, and Y.C. Lin, *Physical characteristics of polyimide films for flexible sensors*, Appl. Phys. A 92 (2008), pp. 693–701.
[5] X. Zhang, L. Hu, and D. Sun, *Nanoindentation and nanoscratch profiles of hybrid films based on (γ-methacrylpropyl)-trimethoxysilane and tetraethoxysilane*, Acta Mater. 54 (2006), pp. 5469–5475.
[6] T.H. Fang, C.I. Weng, and J.G. Chang, *Machining characterization of the nano-lithography process using atomic force microscopy*, Nanotechnology 11 (2000), pp. 181–187.
[7] P. Kizler and S. Schmauder, *Simulation of the nanoindentation of hard metal carbide layer systems – The case of nanostructured ultra-hard carbide layer systems*, Comput. Mater. Sci. 39 (2007), pp. 205–213.
[8] K. Oyeon, *Orientation effects of elastic–plastic deformation at surfaces: Nanoindentation of nickel single crystals*, Mol. Simul. 31 (2005), pp. 115–121.
[9] J. Jin, S.A. Shevlin, and Z.X. Guo, *Multiscale simulation of onset plasticity during nanoindentation of Al(001) surface*, Acta Mater. 56 (2008), pp. 4358–4368.
[10] B. Shiari, R.E. Miller, D.D. Klug, and D. Dennis, *Multiscale simulation of material removal processes at the nanoscale*, J. Mech. Phys. Solids 55 (2007), pp. 2384–2405.
[11] M.A. Tschopp and D.L. McDowell, *Influence of single crystal orientation on homogeneous dislocation nucleation under uniaxial loading*, J. Mech. Phys. Solids 56 (2008), pp. 1806–1830.
[12] Y. Lee, J.Y. Park, S.Y. Kim, S. Jun, and S. Im, *Atomistic simulations of incipient plasticity under Al(111) nanoindentation*, Mech. Mater. 37 (2005), pp. 1035–1048.
[13] S. Kazanc and C. Tatar, *Investigation of the effect of pressure on some physical parameters and thermoelastic phase transformation of NiAl alloy*, Int. J. Solids Struct. 45 (2008), pp. 3282–3289.
[14] Z.H. Hong, S.F. Hwang, and T.H. Fang, *Atomic-level stress calculation and two potentials for critical conditions of deposition process*, Cryst. Growth Des. 8 (2008), pp. 1191–1199.
[15] Y. Qiang, Y. Thurner, T. Reiners, O. Rattunde, and H. Haberland, *Hard coatings (TiN, $Ti_xAl_{1-x}N$) deposited at room temperature by energetic cluster impact*, Surf. Coat. Technol. 100 (1998), pp. 27–32.
[16] J.M. Haile, *Molecular Dynamics Simulation Elementary Methods*, Wiley, New York, 1992.
[17] C.L. Liu, T.H. Fang, and J.F. Lin, *Atomistic simulations of hard and soft films under nanoindentation*, Mater. Sci. Eng. A 452–453 (2007), pp. 135–141.

[18] J.A. Zimmerman, C.L. Kelchner, P.A. Klein, J.C. Hamilton, and S.M. Foiles, *Surface step effects on nanoindentation*, Phys. Rev. Lett. 87 (2001), pp. 165507–165510.
[19] T.H. Fang, W.J. Chang, and C.I. Weng, *Nanoindentation and nanomachining characteristics of gold and platinum thin films*, Mater. Sci. Eng. A 430 (2006), pp. 332–340.
[20] H. Hölscher and B. Anczykowski, *Quantitative measurement of tip-sample forces by dynamic force spectroscopy in ambient conditions*, Surf. Sci. 579 (2005), pp. 21–26.
[21] J.D. Kiely and J.E. Houston, *Nanomechanical properties of Au (111), (001), and (110) surfaces*, Phys. Rev. B 57 (1998), pp. 12588–12594.